



HAL
open science

An innovative approach of surface polishing for SRF cavity applications

Oleksandr Hryhorenko, Claire Z. Antoine, William Magnin, Monish Rajkumar, François Brisset, Stéphane Guilet, David Longuevergne

► **To cite this version:**

Oleksandr Hryhorenko, Claire Z. Antoine, William Magnin, Monish Rajkumar, François Brisset, et al.. An innovative approach of surface polishing for SRF cavity applications. 2023. hal-04024544v1

HAL Id: hal-04024544

<https://hal.science/hal-04024544v1>

Preprint submitted on 9 Feb 2023 (v1), last revised 11 Mar 2023 (v2)

HAL is a multi-disciplinary open access archive for the deposit and dissemination of scientific research documents, whether they are published or not. The documents may come from teaching and research institutions in France or abroad, or from public or private research centers.

L'archive ouverte pluridisciplinaire **HAL**, est destinée au dépôt et à la diffusion de documents scientifiques de niveau recherche, publiés ou non, émanant des établissements d'enseignement et de recherche français ou étrangers, des laboratoires publics ou privés.



Distributed under a Creative Commons Attribution 4.0 International License

An innovative approach of surface polishing for SRF cavity applications

O. Hryhorenko^{1†}, C. Z. Antoine², W. Magnin³, M. Rajkumar³, F. Brisset⁴, S. Guilet⁵,
D. Longuevergne¹

¹Université Paris-Saclay, CNRS/IN2P3, IJCLab, 91405 Orsay, France

²Université Paris-Saclay, CEA, Département des Accélérateurs, de la Cryogénie et du Magnétisme, 91191, Gif-sur-Yvette, France.

³LAM PLAN SA, 7 Rue des Jardins, 74240 Gaillard, France

⁴Université Paris-Saclay, CNRS-IN2P3, ICMO, 91405 Orsay, France

⁵Sorbonne Université, CNRS, INSP, 75005 Paris, France

Abstract

The damage layer produced during the Niobium sheets and cavity fabrication processes is one of the main reasons why cavities have to undergo an extensive surface preparation process to recover optimal superconducting properties. Today, this includes the use of lengthy, costly, and dangerous conventional polishing techniques as buffered chemical polishing (BCP), or electro-polishing (EP). We propose to avoid or at least significantly reduce the use of acids. We developed a novel method based on metallographic polishing of Nb sheets, consisting of 2-3 steps. We demonstrate that this surface processing procedure could be transferred to large dimensions and industrialized thanks to a limited number of steps and its compatibility with standard lapping polishing devices.

Key words

Metallographic polishing; Superconducting radio-frequency cavity; Niobium; Surface Roughness, Damage layer.

INTRODUCTION

Superconducting radio-frequency (SRF) cavity is the key element of linear or circular accelerators where radiofrequency (RF) electromagnetic (EM) fields are used for the acceleration of continuous wave (CW) particle beams, see Figure 1 [1]. The cavity surface material is subject to intense normal-to-surface electric fields (~ 100 s of MV/m) and tangential magnetic fields which induce high surface current density ($\sim 1-100$ s of GA/m²) in the first 100s of nm, as determined by the cavity geometry. Surface currents on the cavity walls are causing dissipations due to the RF surface resistance (indeed, under RF regime superconductors exhibit a non-0 surface resistance but it is about 10⁵ order of magnitude less than copper). Moreover, the crystalline quality of the first 100s of nm of the surface is of paramount importance for the superconducting performance of the material. The SRF cavities require smooth and well-recrystallized surface and need to operate under cryogenic temperatures, typically at superfluid helium temperature, way below the critical temperature of the superconducting material denoted T_c ($T_c \sim 9.2$ K for Niobium) [2].

The abrupt transition from superconducting to a normal state, called quench, is not only determined by the critical temperature but also by the amplitude of the magnetic

field [4]. Above the critical magnetic field H_{c1} , or more specifically, in SRF conditions, above the superheating field H_s [5], the superconductor can be quenched even at cryogenic temperatures [1-2, 4-5].

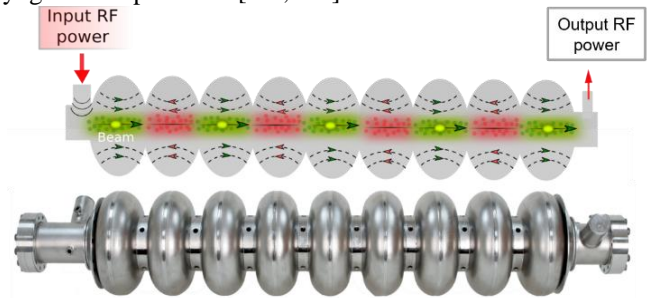


Figure 1: TESLA-shaped a 9-cell elliptical cavity made of Nb operating at 1.3 GHz [3].

Nowadays, the preferred material for SRF cavities fabrication is the Niobium. This choice is driven not only by its high critical temperature ($T_c = 9.2$ K) and high magnetic field of first entry H_{c1} (~ 200 mT) among pure elements but also by its mechanical properties as a metal; workability and weldability. Other superconducting materials, like Nb₃Sn, NbTiN, MgB₂ alloys, have a higher critical temperature but could only be used as thin films on a workable substrate [6-8]. In both cases, the performance of cavities, evaluated in terms of quality factor Q_0 and accelerating field, is significantly impacted by the surface quality in terms of pollution, crystalline structure, and topology [1]. A single microscopic defect such as a microscopic inclusion, scratch, or pull-out becomes a source of local field enhancement and/or heat (normal conducting material) leading to early quench and/or low-quality factor. In order to avoid any reduction of superconducting properties, the surface defects created during Niobium sheet fabrication and cavity manufacturing have to be removed to recover a clean and damage-free surface. The so-called damage layer is of the order of 150-200 μ m [1, 2].

The penetration depth of the electromagnetic field inside the superconducting material is given by the London penetration depth denoted λ_L . Hence, superconducting properties have to be ensured over several hundreds of nanometers for Niobium. Deeper into the material, only good thermal properties are required to ensure efficient heat transport from the RF side to the helium bath side [1-2, 5].

MOTIVATION

Standard mechanical polishing can provide very smooth surfaces but a damage layer (about 100 μm on Nb) is still present at the surface. Buffered chemical polishing (BCP) and electropolishing (EP) are conventional methods used to remove the damaged layer and prepare cavities [9,10]. BCP is composed of acids such as HNO_3 , H_3PO_4 , and HF at a typical 1:2:1 ratio. BCP is a relatively simple and fast technique to remove the damaged layer (~ 4 hours). However, BCP is rather an etching process than polishing, and as a consequence, the final surface roughness is typically worsened because of the differential etching rate versus grain orientation. EP produces smoother surfaces compared to BCP, but this process is more complex (involves the use of an electrode in the mixture of H_2SO_4 and HF acids at 9:1 ratio) and more time-consuming (~ 8 hours). Both methods are very hazardous for operators and exhibit a bad ecological footprint (HF acid). Operational costs of chemical facilities are high because of safety and recycling legislation. Today, these disadvantages become a significant problem because of the increasing demand of SRF units for the future large-scale accelerators (FCC, ILC), see Fig. 2, which require higher performances, higher reliabilities, and higher repeatability to initiate the construction.

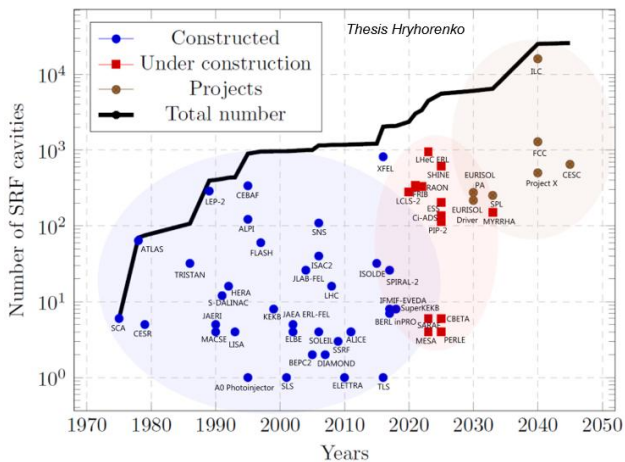


Figure 2: Number of SRF cavities versus year [11].

In order to overcome the aforementioned drawbacks continuous efforts are made in the SRF community to replace or at least significantly reduce the amount of acids [12-21]. Since 1995s, centrifugal barrel polishing (CBP) has been investigated as an alternative mechanical polishing technique applicable to cavities with a revolution symmetry [16]. The decreased surface roughness after CBP in combination with light EP potentially leads to higher accelerating gradient and higher achievable quality factor compared to bulk EP [17-20]. However, the extremely long time of treatment (96-150 hours), the numerous polishing steps (usually 4-5,) and induced mechanical deformations [17], makes CBP not suitable for large-scale production.

In 2009, Calota and al. [22-23] investigated another type of mechanical polishing, called chemical-mechanical polishing (CMP) as a sub-step of metallographic polishing. They proved that CMP in two steps is successful to obtain smoother surfaces compared to conventional polishing, but pre-treatment of the surface is required. Moreover, this study was limited to small samples.

Our study aimed at going farther by developing and optimizing a metallographic polishing procedure transferable to large dimensions (above 10 cm) and integrating a pre-treatment step (lapping). However, contrary to standard chemical polishing and CBP, metallographic polishing can only be applied on flat surfaces. This polishing procedure has thus to be performed directly on Niobium sheets before forming, following an alternative path as depicted in Figure 3. This alternative path can be envisaged as former studies done by Antoine et al. [2] showed that the damaged layer is mainly created during the fabrication process of Niobium sheets. The fabrication of cavities, involving deep drawing and Electron Beam Welding (EBW), are only responsible for a limited damaged layer of a few microns. Further studies are on-going to consolidate these observations but are not reported here.

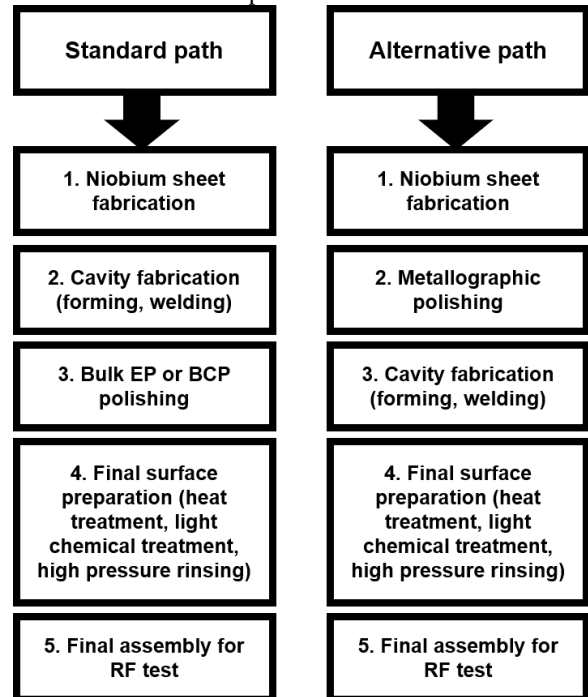


Figure 3: Main steps in cavity life cycle for standard and new suggested procedure.

This paper will be organized as follows. After a brief reminder of the main requirements to produce a SRF-compatible surface, we describe first the alternative metallographic polishing procedure developed on small samples. Secondly, we show how this procedure has been transferred to large dimensions. Finally, we discuss the results and conclude.

REQUIREMENTS FOR SRF SURFACE PROCESSING

To ensure optimal superconducting properties and to make the surface processing procedure compatible with industrialization constraints, the following requirements can be specified:

- Material removal between 150-200 μm to suppress the damaged layer created during Niobium sheet fabrication.
- Preserve SRF properties over the first hundreds of nanometers: After final step, crystalline defects and pollution (embedded abrasives) should be removed.
- To be competitive, the duration of treatment should be comparable to standard chemical techniques (of the order of one working day)
- Limit the number of polishing steps to 2 or 3 steps (instead of 5 or 6 steps typically required in standard metallographic polishing recipes) [24]
- Polishing technique should be transferable to large dimensions.

PROCEDURE AND SURFACE ANALYSIS ON SMALL SAMPLES

Flat samples of different dimensions were prepared from a 4.1-mm-thick sheet of high-purity polycrystalline Niobium (RRR=300). Two different types of samples with different initial surface states have been used in this work as depicted in Figure 4. One set of samples has been treated by BCP (150 μms of removed material) to ensure that any alteration of the quality (pollution, strain, topology) is only caused by MP surface processing. The second set of samples corresponds to samples “as received”. These samples aim at characterizing the efficiency of MP processing to remove the damaged layer created during Niobium sheet fabrication.

All samples undergo before and after metallographic polishing a cleaning cycle consisting of the following steps:

- rinsing with deionized water,
- cleaning with deionized water at 30 °C in ultrasonic bath,
- drying with Nitrogen flow,
- cleaning with ethanol.

Surface processing has been performed on a commercial lapping polishing device MASTERLAM 1.0 manufactured by the French company LAM PLAN [25] as shown in Figure 5. This machine is an automatic device equipped with an oscillating arm pressing the rotating sample holder on the rotating polishing disk support with a diameter of 300 mm giving the possibility to polish samples up to $\phi 150$ mm.

The polishing parameters such rotation speeds (disk/sample holder), direction of rotation (clockwise/counter clockwise), applied pressure, type and size of abrasives were studied and have been discussed in [11].

The rotational speeds of the sample holder and the polishing disk support were set to 150 rotations per minute (RPM). The lapping/polishing disk and samples were rotated both in the clockwise direction. Moreover, the device was used in an oscillating mode leading to more uniformly distributed abrasives on the samples/disk. In this study, we describe the optimized polishing protocol consisting of two steps. More information on how the process has been optimized can be found in [11].

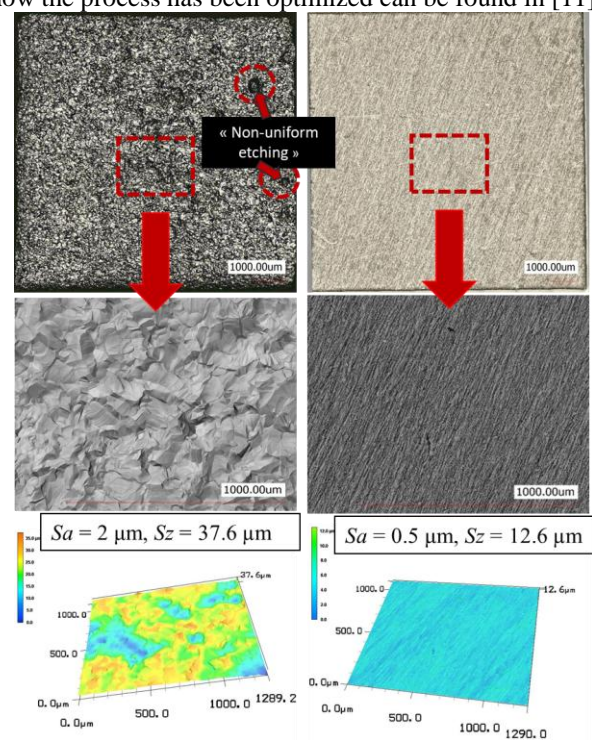


Figure 4: Optical and 3D images acquired by a laser confocal microscope (Keyence VKX200) for BCP-treated samples (left) and “as received” samples (right).



Figure 5: Picture of the polishing device MASTERLAM 1.0 from LAM PLAN.

Step 1: lapping step

A rigid composite disk (RCD) made of Cu powder and resin (commercial name CAMEO Gold) in combination with 3 μm polycrystalline diamonds (dia.) is used as a first step. This step aims at planarizing the surface and removing the initial damaged layer caused during fabrication (150-200 μm). We evaluated the material removal rate (MRR) for different applied pressures (See Figure 6). As expected, the measured MRR is proportional to the applied pressure.

To maintain a constant MRR over time, it is essential to proceed with a continuous supply of abrasives and use disks with a meshed structure acting as an efficient path to remove debris. Hence, as depicted in Figure 7, the damaged layer created during Nb sheets fabrication could be removed within 0.5-4 hours depending on the applied pressure.

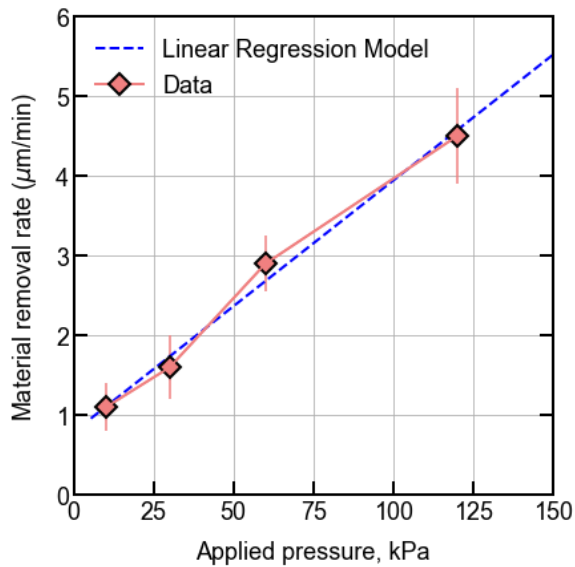


Figure 6: Evolution of material removal rate versus applied pressure during lapping step.

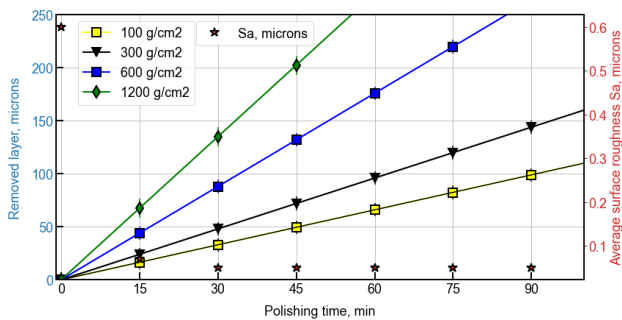


Figure 7: Evolution of removed layer and roughness versus time during the lapping step. Note: the left vertical axis applies to solid-line curves.

After Step 1, surface roughness was examined by a laser confocal microscope. The average surface roughness (S_a) and the maximum height fluctuation of the surface

profile (S_z) are measured. After planarization, as depicted in Figure 8, a mirror finish surface with $S_a = 0.05 \mu\text{m}$ and $S_z = 3.11 \mu\text{m}$ has been obtained. However, at this stage, after this very aggressive step, the presence of significant crystalline damages and embedded abrasives can be reported. To qualify the depth and density of such pollution and to reveal hidden artifacts, additional processes such as CMP or BCP etching can be performed as surface diagnostics. CMP, as a very soft surface treatment, reveals any surface pollution embedded underneath the surface. As shown in Figure 9, after 15 minutes of CMP, the surface appears to be strongly polluted by embedded diamonds. On the other hand, BCP tends to reveal crystalline damages because of the differential etching depending on crystalline orientation and imperfections [2]. As depicted in Figure 8, after a short soaking in BCP solution, the polycrystalline structure is reappearing but with intra-grains patterns, signs of residual strains and defects [2, 13].

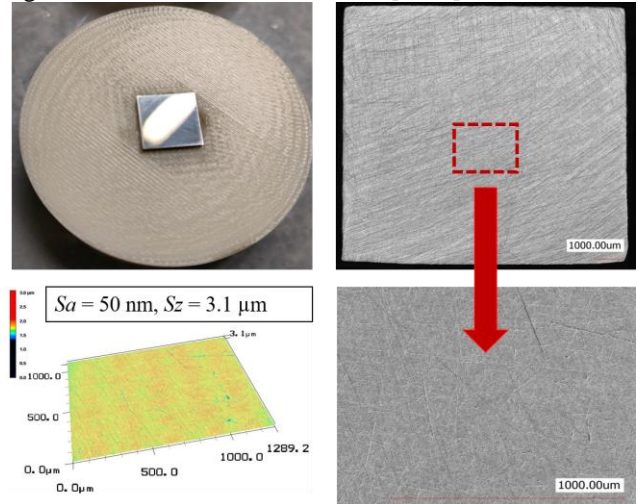


Figure 8: Optical images and 3D images acquired by a laser confocal microscope of a Nb sample after step 1.

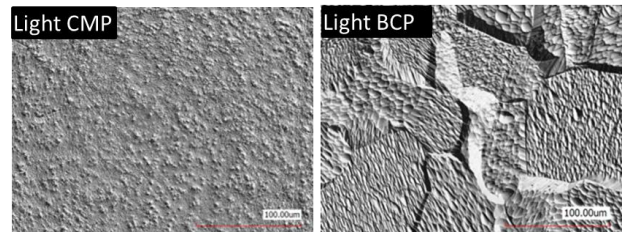


Figure 9: Optical images acquired by laser confocal microscope after step 1 followed by a 15-minute CMP polishing (left), and after a 10-minute BCP etching (right).

As a conclusion for this first step, the lapping step described appears to be a good compromise between removal rate and induced pollution and defects. The removal rate is significantly exceeding the capabilities of conventional chemical treatment. It makes this treatment very efficient to remove the initial damaged layer. However, this step induces a new damaged/polluted layer which will have to be removed by the subsequent polishing step. A precise measurement of the depth of this

induced damaged layer is difficult to perform. Preliminary analysis showed embedded abrasives are within a few microns, but sub-grain damages tend to extend over several tens of microns [13, 26]. An investigation of the residual damaged layer remaining after the final polishing step will be presented below.

Step 2: depollution step

Plain microporous polyurethane cloth (commercial name 4MP1) in combination with 50-nm silica colloidal (SiO_2), hydrogen peroxide (H_2O_2), and ammonia (NH_4OH) diluted in deionized water (up to 20%) is used as a second polishing step. This polishing step, as was mentioned earlier, called CMP, is needed to recover SRF surface properties by removing surface damages (scratches, pull-outs...) and embedded particles caused by Step 1. Step 2 was interrupted every 15 minutes to investigate surface evolution with a confocal microscope (see Figure 10). Silica colloidal solution is efficient to reduce the amount of embedded abrasives versus time. To describe statistically the number of embedded particles, the edge detection algorithms [27, 28] have been applied to the images in Figure 9, and the output of that image recognition is shown in Figure 11. It is shown in Figure 12, that to reduce the level of pollution from thousands to a few particles, Step 2 is required to be at least 2 hours.

However, as can be seen in Fig. 10, a long polishing run causes the re-appearance of the grains, which eventually leads to a roughness increase as depicted in Figure 13. The final surface state of the sample after complete depollution is shown in Figure 14. Hence, Step 2 is not efficient in reducing surface roughness, but efficient in improving the micro-structure and chemical purity of the material. To verify the previous statement, the processed surface has to be verified under RF and at cryogenic temperatures. The first samples were tested at SLAC on a dedicated test bench. Test results have been published in [13] and were not really satisfactory because of Q-disease: the presence of a significant amount of hydrogen in Niobium material leads to the formation of Niobium hydride precipitates when exposed to low temperatures typically between 50K-150K [29]. These Niobium hydrides are non-superconducting and lead to a strong degradation of the surface resistance [29-31]. Thus, the triggering of Q-disease on our samples made the evaluation of the impact of the polishing procedure on the surface resistance not relevant.

Before producing a new sample for the RF test at cryogenic temperature, we proceeded with additional studies on Q-disease after the metallographic procedure which results will be discussed later in this paper.

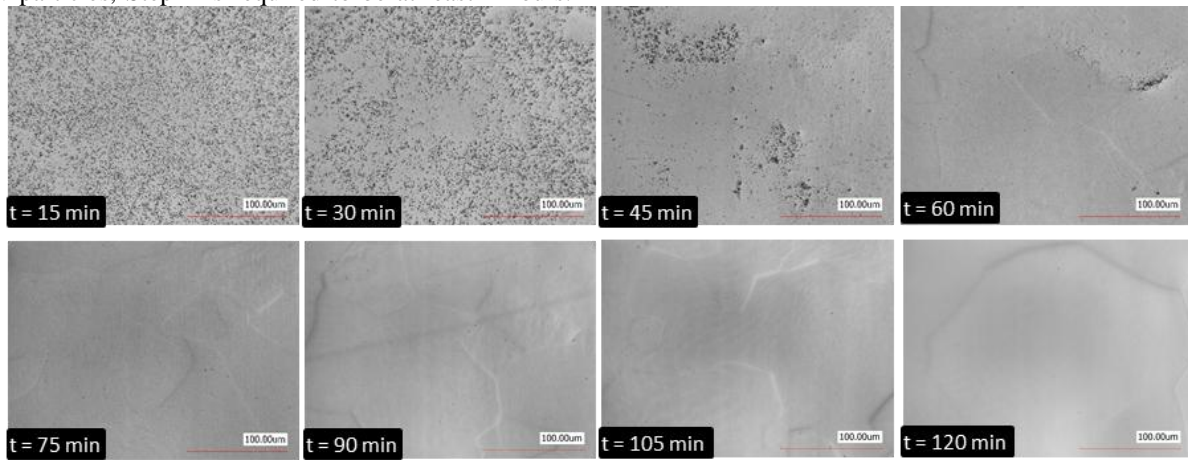


Figure 10: Laser confocal images of Nb surface during Step 2 for different processing duration. Note: imaging depicts the pollution removal, grain appearance, and grain growth.

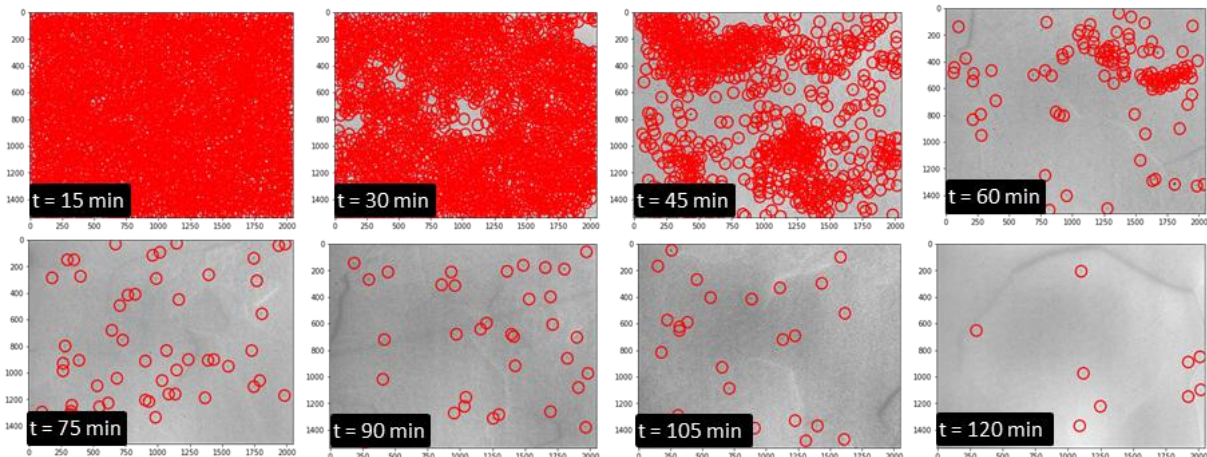


Figure 11: Identified particles from the laser confocal images (Figure 6) with edge-detection algorithms (OpenCV). Red circles correspond to locations where there are embedded diamonds. Scale is defined in pixels.

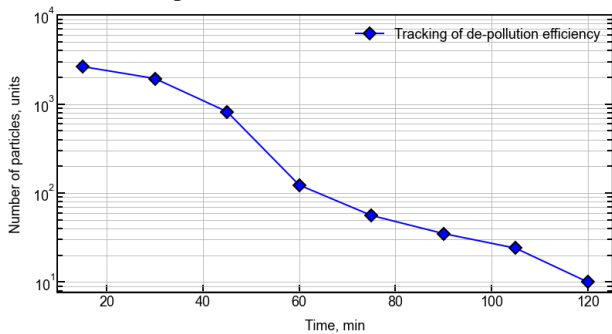


Figure 12: The calculated number of embedded particles versus polishing time.

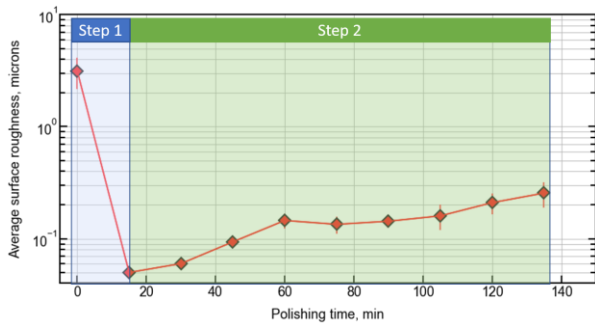


Figure 13: Evolution of the average surface roughness as a function of time.

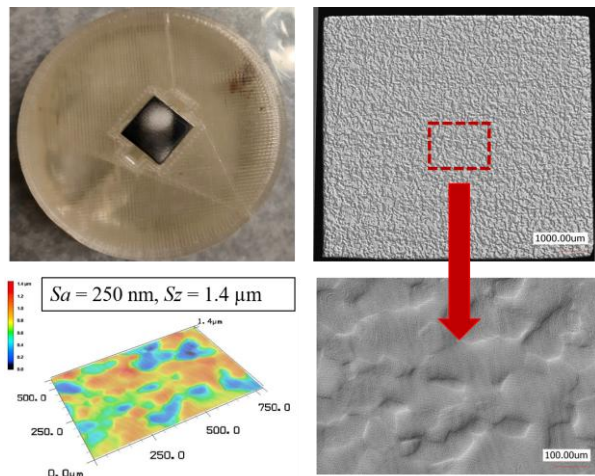


Figure 14: Laser confocal images, optical image, and topography of the Nb sample after step 2.

FINAL SURFACE ANALYSIS ON SMALL SAMPLES

As mentioned earlier, the best way to evaluate surface quality after metallographic polishing is to measure surface resistance under radio-frequency waves at cryogenic temperatures. However, this type of test is expensive, technically difficult, and shows a very low availability [32-35]. The final optimization of polishing parameters is not possible by proceeding with

an iterative approach using such devices. The use of surface characterization techniques sensitive to pollution and crystalline structure within the penetration depth of the RF wave, meaning a few hundreds of nanometres, is required.

In that sense, the use of a scanning electron microscope (SEM) at low voltage (~2kV) with standard detectors like SE (Secondary Electron), BSE (Back-Scatter Electron) and In-Lens (SE detector integrated in SEM column) give a good qualitative assessment of surface pollution and crystalline effects. To address more precisely and quantitatively the crystal quality, advanced analysis like EBSD (Electron Back-Scatter Diffraction) has been used. XPS (X-rays Photo-electron Spectroscopy) and SIMS (Secondary Ion Mass Spectroscopy) were also used to assess surface pollution. Finally, hydrogen content has been investigated indirectly by triggering on purpose the Q-disease and observing the subsequent residual patterns.

EBSD analysis

EBSD scans of the polished face were performed. The polished surface has been analyzed directly by EBSD without any subsequent surface treatment. As this technique is sensitive to the first tens of nanometers [36], it makes it relevant to address the quality of crystalline structure within the RF penetration depth.

As depicted in Figure 15, this 2-step polishing technique does not induce significant crystalline damages. Step 2 is thus efficient and sufficient to remove crystalline damages induced by step.

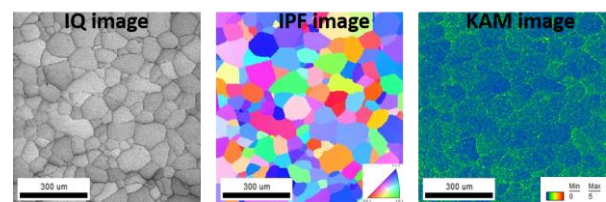


Figure 15: Measured EBSD outputs map of the polished face: a) image quality, b) inverse pole figure, c) kernel average misorientation.

To analyze the quality of the microstructure, we used three maps extracted from EBSD analysis: IQ (image quality), KAM (kernel average misorientation), and IPF (inverse pole figure). IQ gives information about any surface features (patterns quality, grain, grain boundaries, eventual defects, ...). IPF images show that samples are polycrystalline, and depict the orientation of each grain. According to this analysis, the fully random grain orientation indicates no distinct texture after polishing (no colour is predominant) and the complete diffraction of electrons shows that the polishing procedure doesn't create significant damages. KAM gives an estimation of the level of local

dislocation density. This value varies from 0° to 5° in correspondence to colour which indicates the density of the dislocations. The colour code indicates the following:

- Blue – no dislocation,
- Green – minor dislocation,
- Red – significant dislocation.

As can be seen from figure 15, KAM image indicates that the polished face shows only minor dislocation, showing that the surface is almost strain free.

SIMS and XPS Analysis

In an effort to evaluate more precisely the level of surface contamination after the developed metallographic polishing procedure, we used two surface characterization methods, namely SIMS and XPS and compared results to reference samples.

SIMS stands for secondary electron mass spectrometer and is used for chemical composition evaluation. Analysis was performed on a Compact SIMS manufactured by Hidden Analytical company [37] in two different modes: static and dynamic. The static mode gives a global overview of all isotopes between 0 and 200 amu. The dynamic mode allows to measure the evolution of defined masses in depth. In both cases and in our configuration an ion beam of Ar^+ at an energy of 5kV and at a current of 350 nA is used to sputter an area of $2000 \times 2000 \mu\text{m}^2$. Sputtered ions are analyzed by a quadrupole analyzer. In such configurations, the mass spectrum was measured and collected during the first minute of analysis, which corresponds to an estimated depth of few nanometers (sputtering rate is of about 1.5 nm/m

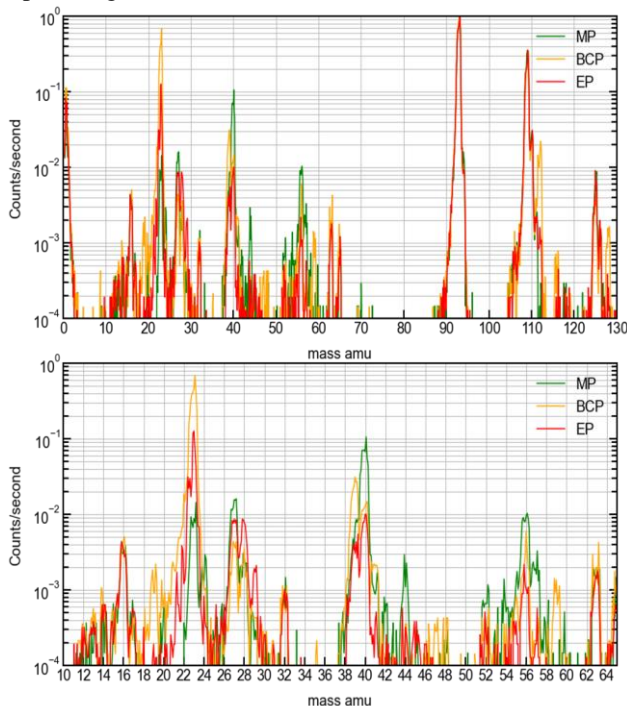


Figure 16: Mass spectrum for three types of the samples MP (green), BCP (orange) and EP (red).

<i>Mass</i>	<i>Positive species</i>
1	H^+
12	C^+
13	CH^+
14	$\text{CH}_2^+, \text{N}^+$,
15	CH_3^+
16	$\text{O}^+, \text{CH}_4^+$
23	Na^+
27	$\text{Al}^+, \text{C}_2\text{H}_3^+$
28	$\text{Si}^+, \text{CHNH}, \text{CO}, \text{N}_2^+, \text{C}_2\text{H}_4$
39	$\text{K}^+, \text{C}_3\text{H}_3^+$
40	$\text{Ca}^+, \text{Ar}^+, \text{CH}_2\text{CN}^+$
44	SiO^+
45	$\text{SiOH}^+, \text{Sc}^+, \text{C}_2\text{H}_5\text{O}^+$
56	$\text{Fe}^+, \text{Si}_2^+$
57	$\text{FeH}^+, \text{C}_4\text{H}_9^+, \text{CaOH}^+$
63	$\text{Cu}^+, \text{ClSi}^+, \dots$
93	$\text{Nb}^+, \text{C}_3\text{F}_3^+, \text{C}_7\text{H}_9^+$
109	NbO^+
125	NbO_2^+

Table 1: Main observed Ions and Fragment Species in SIMS spectra recorded on Niobium after different surface processing (MP, BCP, EP).

The measured mass spectrums of the sample after metallographic polishing in comparison to the reference samples (after BCP and EP) are presented in Fig. 16. Spectrums have been normalized to the highest peak (Nb) allowing to quantitatively define the pollution level after different treatments. SIMS analysis of all samples identified presence of common pollution as listed in Table 1. Above mass 70, the MP spectrum is identical to EP spectrum. However below mass 70, as highlighted in Fig. 16, MP mass spectrum is showing higher pollution but limited for several masses as Si and SiO (due to last polishing step) and stainless-steel compounds. Hence, in order to study the evolution of the species of interest, the depth profiles were acquired and are presented in Appendix. These show pollution limited to the near surface within 10

minutes of analysis corresponding to few tens of nanometers.

So as to complete and consolidate the SIMS observation, we used XPS analysis. X-Ray photoelectron spectroscopy (XPS) analysis was performed with a test-bench at INSP-CNRS laboratory using a monochromatic Al-K α radiation source at 1486.6 eV [38]. In the analysis chamber, vacuum was kept at the level of about 10⁻¹⁰ mbar.

Measured XPS spectra are presented in Figure 17. The survey spectra are calibrated to the hydrocarbon impurity C 1s at 284.8 eV. There are visible peaks for O 1s, Nb 3s, Nb 3p1/2, Nb 3p3/2, C 1s, Nb 3d3/2, Nb 5d3/2, Nb 4s and Nb 4p. The main peaks of interest are O 1s, C 1s and Nb 3d, for which high resolution spectrums were measured. Surprisingly, contrary to SIMS analysis, no photoemission signals of Si particles were observed in spectra.

In order to analyze data and deconvolute the Nb 3d peak, CasaXPS software is used [39]. The reference data of each initial peak position is taken from NIST X-Ray Photoelectron Spectroscopy Database [40]. The final binding energy for each peak position and width were determined using the GL (30) function after subtraction of the background using a Shirley method [41, 42]. The

core-level peak features for metal Nb 3d and Nb 3d oxides were decomposed as doublets with a spin-orbital splitting of 2.7 eV, 2.8 eV and 2.8 eV for MP, BCP and EP treated samples respectively. Nb 3d peaks were de-convoluted on the following compounds: Nb₂O₅, NbO₂, NbO, NbC, see Figure 18. The detailed surface composition of each sample is presented in Table 2.

Several statements can be made based on high-resolution XPS spectra. The surface concentration of the pentoxide after MP is reduced from 82.55% (BCP) down to 73.07% (MP), but this thickness would not affect the cavity performance as it is a dielectric layer. However, the increase of other types of oxides will affect the performance, as they might increase the losses. The maximal content of the NbO compound is slightly increased from 6.43% (EP) to 7.6% (MP). At this stage, the oxide layer composition is not primordial as Nb cavities are typically heat treated above 650°C at the end of the fabrication process to degas the hydrogen and avoid the so-called Q-disease.

Finally, MP shows a compatible content of Carbon compared to conventional treatment, which confirms that polishing abrasives from step 1 are efficiently removed, and shows good agreement with optical and SIMS analysis.

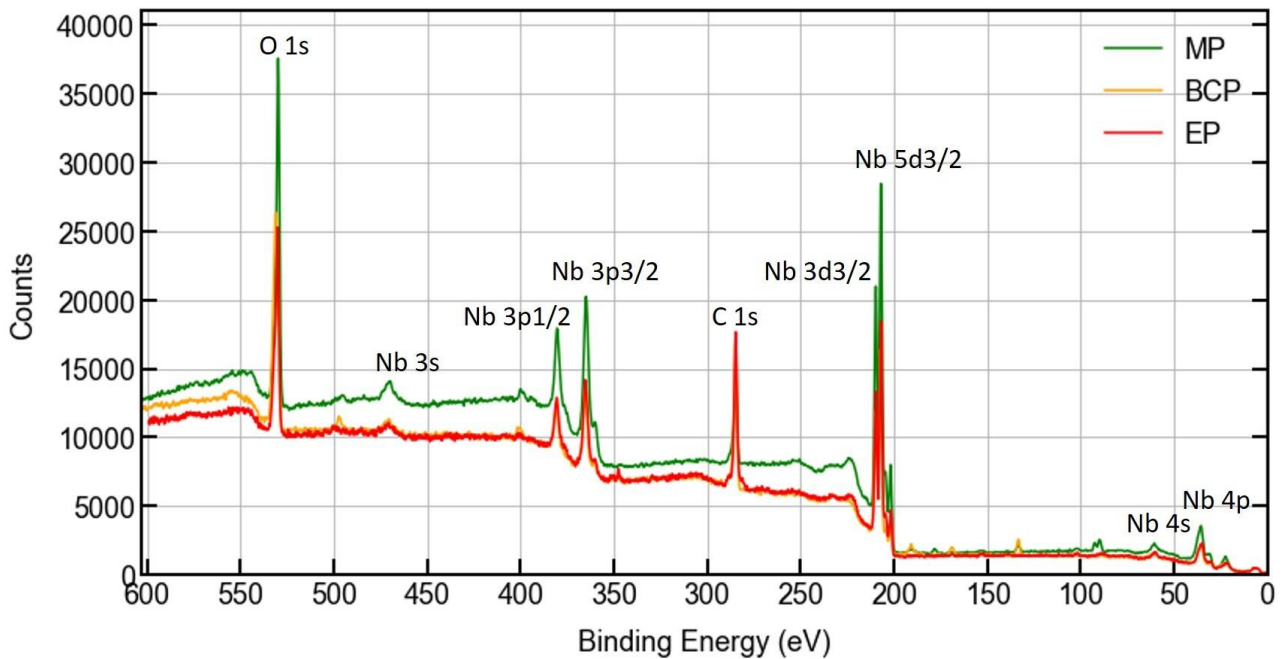


Figure 17: XPS survey spectra of Nb samples after MP, BCP, and EP treatment, calibrated with C 1s position at BE 284.8 eV.

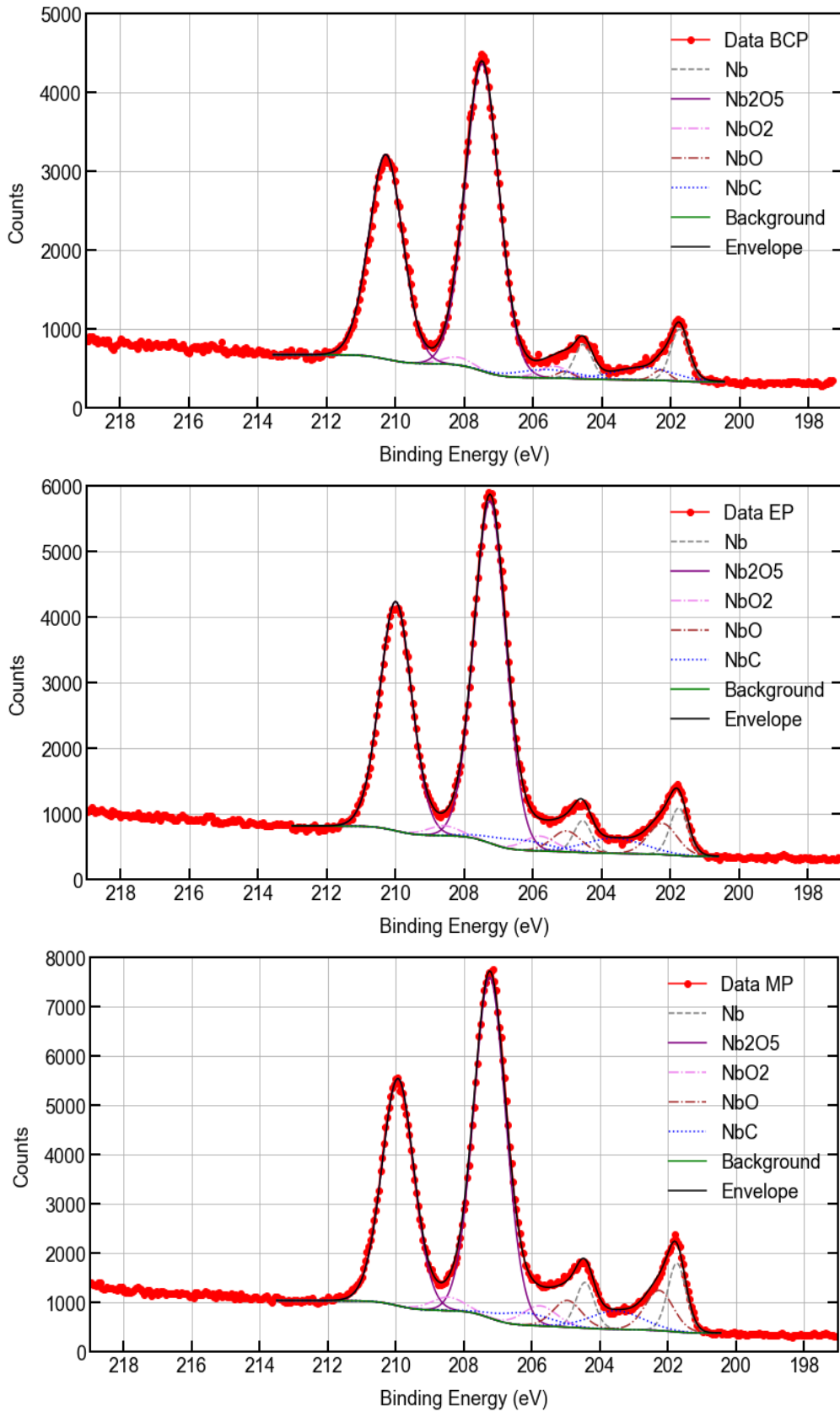


Figure 18: High resolution XPS spectra for the Nb 3d core peak after different treatments (BCP, EP and MP).

Table 2: Composition and chemical states after different polishing treatments (BCP, EP & MP).

Polishing	Element	Composition and chemical states					
			Nb ₂ O ₅	NbO ₂	NbO	Nb	NbC
BCP	Nb 3d5/2, Nb 3d3/2	B.E. [eV]	207.48, 210.28	205.39, 208.19	202.27, 205.07	201.74, 204.54	202.79, 205.59
		FWHM [eV]	1.16	1	0.55	0.61	2.04
		Area [%]	82.55 ↑	2.75 ↓	1.35 ↓	7.38 ↓	5.97≈
EP	Nb 3d5/2, Nb 3d3/2	B.E. [eV]	207.24, 209.99	205.8, 208.6	202.22, 205.02	201.75, 204.55	203.63, 206.43
		FWHM [eV]	1.09	1.08	0.99	0.61	2.02
		Area [%]	77.82 ↑	3.31 ↓	6.43 ↓	6.03 ↓	6.4≈
MP	Nb 3d5/2, Nb 3d3/2	B.E. [eV]	207.23, 209.93	205.76, 208.46	202.25, 204.95	201.73, 204.43	203.52, 206.22
		FWHM [eV]	1.11	1.17	0.98	0.63	1.8
		Area [%]	73.07 ↓	4.51 ↑	7.6 ↑	8.38 ↑	6.43≈

Q-disease analysis and mitigation treatments

Surface treatments as BCP, EP and MP cause the pollution of the bulk Nb with hydrogen interstitials [44-47]. This scenario leads to poor cavity performance due to precipitation of Niobium hydrides at low temperature inducing the creation of irreversible surface defects called “H-footprints”. This phenomenon, named Q-disease or 100K-effect in SRF community, is generally mitigated by degassing hydrogen in a vacuum furnace between 600 and 800°C. In our case, we triggered on purpose Q-disease to qualitatively evaluate hydrogen contamination of our samples. Laser confocal microscope was used to observe the creation or absence of H-footprints on the surface before and after 10-hour soaking in liquid Nitrogen. This rough method is only sensitive to irreversible crystal damages remaining after warming up in the case of a very strong hydrogen contamination. The non-appearance of footprints is not a sign of non-contamination. Moreover, the surface quality has to be good enough to be able to observe the H-footprints. Indeed, after the first polishing step, no footprints could be observed although Niobium is known to be highly contaminated after a lapping process.

Figure 19 shows the results of the Q-disease tests after MP treatment. After the full MP process, we observe a significant density of H-footprints on the surface, proof of strong hydrogen contamination. This contamination could be due to the polishing process or even previous steps (Niobium fabrication, cutting). In an effort to discriminate if the last polishing step is responsible for hydrogen loading, we degassed the sample at 600°C for 10h under vacuum and applied an additional “step-2” polishing. No H-footprints are visible after heat treatment nor after additional mechanical polishing with colloidal silica.

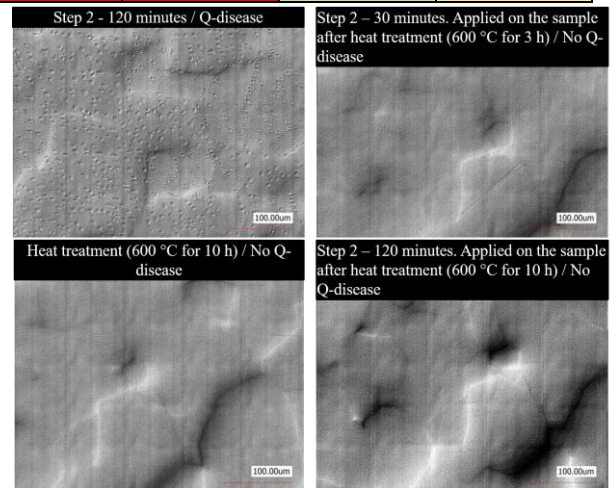


Figure 19: Photographs of Niobium surface after nitrogen soaking after a full MP process (upper left), after heat treatment (bottom left) and additional step-2 polishing (upper and bottom right).

TRANSFER TO LARGE DIMENSIONS

In order to polish Niobium disk dimensions compatible with 1.3 GHz cavity fabrication (260 mm in diameter), the polishing procedure was adapted and optimized for larger lapping devices. For this study, we used the device MM.9100S fabricated by and in operation at LAM PLAN company (Figure 20) [25]. The large rotating disk with a diameter of one meter and the three independent pistons give the possibility to polish simultaneously three Niobium disks. Several issues were faced as device parameters and consumables types differ due to the size difference between metallographic and lapping devices. Firstly, it was impossible to apply the same pressure on samples and large disks during **Step 1**. As a consequence, to compensate for the reduction of MRR, the grain size of

diamonds had to be increased from 3 μm to 6 or 9 μm . Secondly, as rigid composite disk used for small samples are not available for lapping device, an alternative and equivalent lapping disk had to be identified.



Figure 20: Photograph of the polishing machine MM.9100S in operation at LAM PLAN company.

Optimization of Step-1 for large disks

The following types of disks were tested: cast iron, synthetic fiber, and patented disk (LAM PLAN NEW LAM M'M' GREEN). Cast iron in combination with SiC is widely used in industrial applications because of very efficient stock removal, but in the case of Nb, the material tends to be heavily scratched, see in Fig. 21. The synthetic fiber in combination with dia. of 9 μm shows good results in terms of final roughness, but not sufficient enough in terms of material removal rate. Moreover, the surface quality was not uniform even after 1 hour as shown in Figure 19. Finally, the patented disk LAM PLAN NEW LAM M'M' GREEN [25], integrating a meshed structure made of soft and hard material, shows homogeneous polishing over the whole surface, with acceptable removal rate. The disk could be used either with diamonds of 6 μm or 9 μm . Table 3 summarizes the different MRR depending on the applied pressure and polished area.

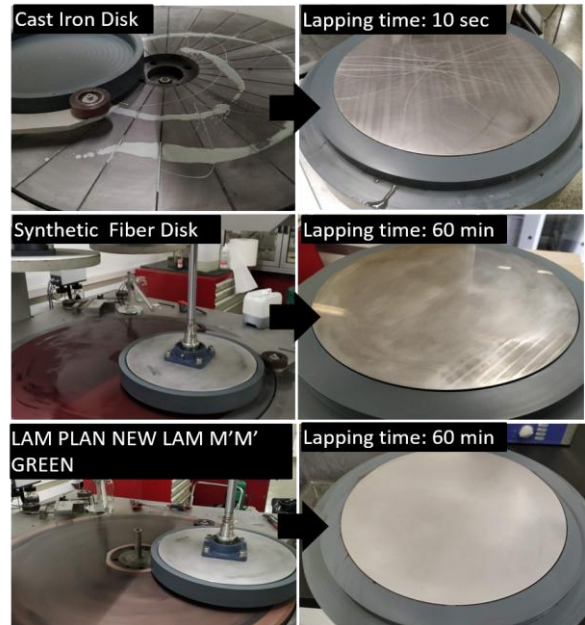


Figure 21: Photographies of the tested lapping disks (left) and surface quality of Niobium disks after Step 1 (right).

Table 3: Measured removal rate (MRR) for different polishing configurations.

Area, cm^2	Pressure, g/cm^2	Disk type + diamonds, μm	MRR, $\mu\text{m}/\text{min}$
1	1200	CAMEO Gold + 3	4.5 \pm 0.6
1	600	CAMEO Gold + 3	2.9 \pm 0.4
1	300	CAMEO Gold + 3	1.6 \pm 0.4
1	200	CAMEO Gold + 3	1.1 \pm 0.3
125	100	CAMEO Gold + 3	0.6 \pm 0.1
530	200	New Lam M'M' Green + 6	1 \pm 0.1
530	200	New Lam M'M' Green + 9	1.5 \pm 0.1

Optimization of Step-2 for large disks

The main issue observed for this polishing step was the non-uniformity of surface quality when using a standard plain polishing pad. Indeed, the apparition of 2 types of regions (we defined as ‘bright’ and ‘dark’) were observed after one hour of polishing. Laser confocal observations of ‘bright’ spots, see Fig. 22, revealed a large concentration of embedded diamonds, whereas ‘dark’ spots showed a very limited contamination. This problem was solved, as in a previous study for RF disks of 13 cm-diameter [11], by using a meshed polishing pad (See Figure 23). This non-uniformity during the depollution process was explained by a non-optimal distribution of liquid over

the polishing pad. The final surface results are presented in the following section.

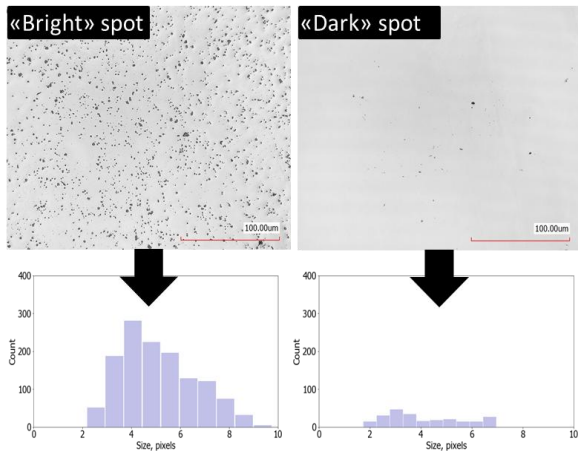


Figure 22: Top - Laser confocal images of bright (left) and dark (right) spots after 60 minutes of polishing. Bottom – calculated distribution of abrasives for bright (left) and dark (right) spots.

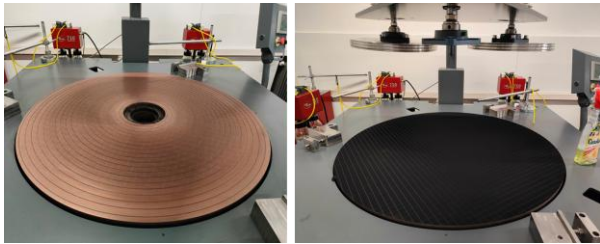


Figure 23: Photograph of lapping disk (left) and meshed polishing pad (right).

Final surface analysis of large disk

The surface of the polycrystalline Niobium disk has been checked after 2 hours of silica colloidal polishing with a laser confocal microscope at three different radii (See Fig. 24). Pictures in Figure 25 confirm the efficiency of step 2 to remove embedded particles over the whole surface. Moreover, a final average roughness of $Sa = 0.2 \mu\text{m}$ has been measured. At the sight of disk dimension, no advanced surface analysis as for small samples could be performed. We don't expect any major differences as polishing parameters and consumables used are very similar to the one used for small samples.

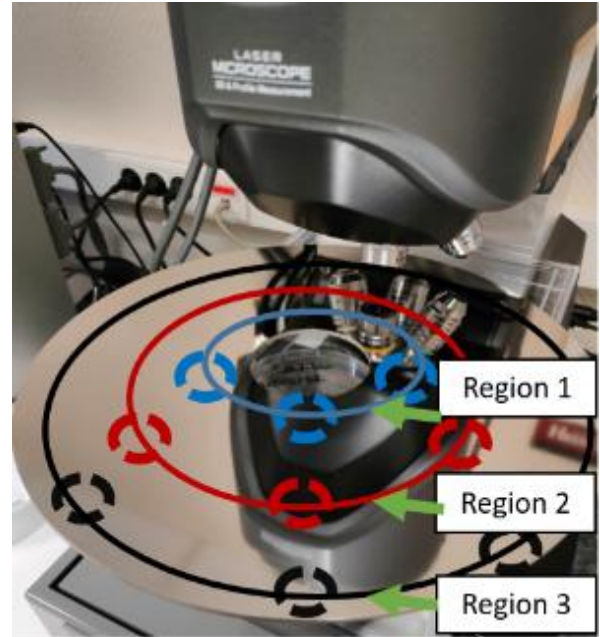


Figure 24: Photograph of polished Nb disk with indicated regions which were analyzed with a laser confocal microscope. Note: polishing time 2 hours.

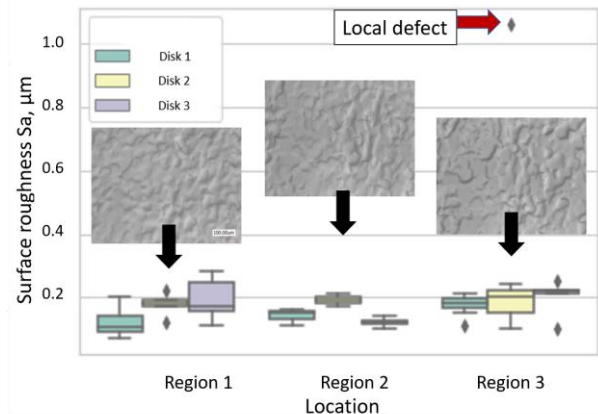


Figure 25: Measured surface roughness at three different radii. Region 1 – inner edge, Region 2 – center, and Region 3 – outer edge.

CONCLUSION

We developed an alternative and a simple 2-step polishing process to first, efficiently remove the damaged layer and, secondly, improve the surface quality of Niobium to meet the stringent requirements for superconducting accelerating cavities. Not only roughness, but also surface purity and crystalline structure are of first importance to ensure good superconducting properties. The technique was first developed on small samples. Extensive surface analysis at room temperature as SIMS, XPS and EBSD have been performed and demonstrated a very acceptable surface quality. Additional tests at cryogenic temperature will be performed to evaluate the surface

resistance under radiofrequency wave. The availability of such devices capable of resolving residual resistances as low as few nano-Ohms is very low. This work is still in progress and results will be published in a future paper.

The compatibility of this technique for large disks has then been demonstrated. The procedure uses non-fixed diamonds between 3 μm and 9 μm depending on the sample dimensions, followed by a depollution step involving colloidal silica during at least 2 hours to reach a good homogeneity all over the surface. The final roughness obtained, because of depollution requirements, is not optimal but is similar to the one achieved by EP. This technique is promising not only for bulk Nb, but also for substrate preparation (Nb, Cu...) for future thin-film deposition. However, the fabrication of a complete 1.3 GHz single-cell cavity by this alternative path has to be demonstrated. Dedicated studies in collaboration with KEK are in progress.

ACKNOWLEDGEMENTS

We are very grateful and appreciate the support from the members of LAM PLAN team. Especially we thank

William MAGNIN and Monish RAJKUMAR for the supporting assistance connected with the lapping and polishing tasks. Also, we would like to express our deepest thanks to S. GUILLET (INSP/CNRS-IN2P3) for the invaluable assistance in the XPS analysis. Part of this work was supported by the European Nuclear Science and Application Research-2 (ENSAR-2) under grant agreement N° 654002.

APPENDIX

Depth profile analysis was carried out based on the chosen masses with a continuous sputtering by Ar⁺ beam. In the oxide layer, see Fig. 26, the signals of masses 27, 40, 44, and 109 are slightly higher in the case of the MP polished samples. At the moment when the oxide layer is over, the situation is contrary and signals are lower. It might be due to the fact that MP brings fewer hydrocarbons to the surface than conventional treatment.

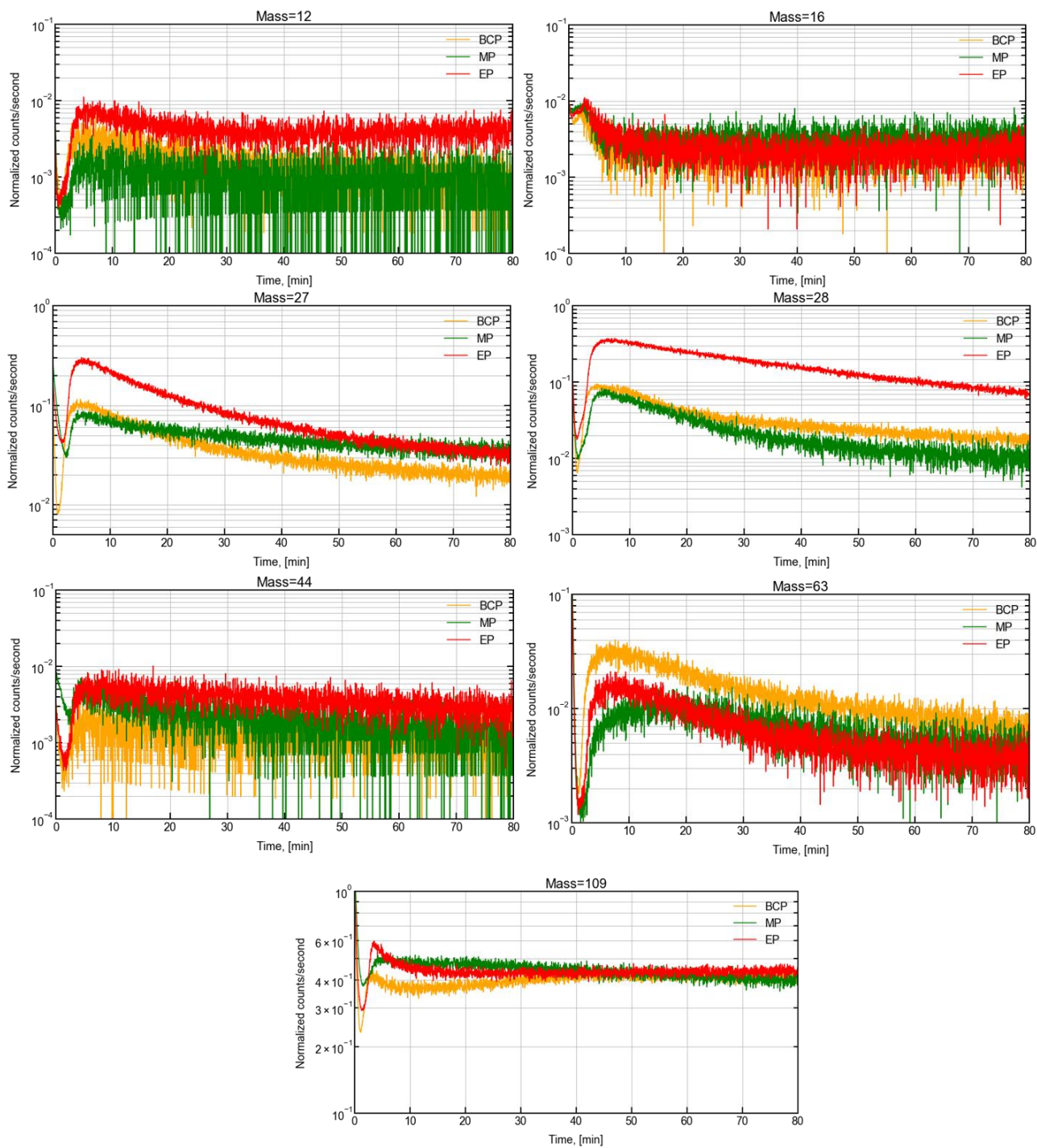


Figure 26: SIMS comparison of depth profiles after metallographic polishing (MP), buffered chemical polishing (BCP), and EP (electro-polishing) measured for desired investigated mass.

REFERENCES

- [1] H. Padamsee, "RF Superconductivity," Mar. 2009, doi: 10.1002/9783527627172
- [2] Antoine, Claire. Materials and surface aspects in the development of SRF Niobium cavities. No. EuCARD-BOO-2012-001.2012.
- [3] O. Hryhorenko et al. "Alternative surface processing pathway to the future large-scale facilities". French-Ukrainian workshop 2021, Orsay, France, 2021.
- [4] C. Z. Antoine, "Material and surface aspects in SRF technology", Gif-sur-Yvette, France, 2018.
- [5] Hasan Padamsee, Jens Knobloch, Tom Hays, et al. RF superconductivity for accelerators. Vol. 2011. Wiley Online Library, 2008.
- [6] A. Gurevich, "Enhancement of rf breakdown field of superconductors by multilayer coating", Appl. Phys. Lett. 88, 012511 (2006), <https://doi.org/10.1063/1.2162264>.
- [7] Junginger, T., Prokscha, T., Salman, Z., Suter, A., & Valente-Feliciano, A. M. (2018). Critical fields of SRF materials. In S. Koscielniak, T. Satogata, V. R. W. Schaa, & J. Thomson (Eds.), International particle accelerator conference: Vol. 9. Proceedings of the 9th international particle accelerator conference (pp. 3921-3924). <https://doi.org/10.18429/JACoW-IPAC2018-THPAL118>.
- [8] Tajima, Tsuyoshi, Hitoshi Inoue, Leonardo Civale, Jiquan Guo, Christopher S. Yung, Thomas Proslie, Michael J Pellin, Akiyoshi Matsumoto, E. Watanabe and Binping Xiao. "MgB2 THIN FILM STUDIES." (2011).
- [9] H Diepers et al. "A new method of electropolishing niobium". In: Physics Letters A 37.2 (1971), pp. 139-140.
- [10] Gianluigi Ciovati, Hui Tian, and Sean G Corcoran. "Buffered electrochemical polishing of niobium". In: Journal of Applied Electrochemistry 41.6 (2011), pp. 721-730.
- [11] O. Hryhorenko, "Development and optimization of mechanical polishing process for superconducting accelerating cavities", PhD thesis, Université Paris-Saclay, 2019.
- [12] C. Z. Antoine and R. Crooks, "Reducing Electropolishing Time with Chemical-Mechanical Polishing", in Proc. 14th Int. Conf. RF Superconductivity (SRF'09), Berlin, Germany, Sep. 2009, paper TUPPO071, pp. 405-405.
- [13] O. Hryhorenko, C. Z. Antoine, M. Chabot, and D. Longuevergne, "Metallographic Polishing Pathway to the Future of Large Scale SRF Facilities", in Proc. 19th Int. Conf. RF Superconductivity (SRF'19), Dresden, Germany, Jun.-Jul. 2019, pp. 828-832.
- [14] A-M. Valente-Feliciano, H. L. Phillips, S. Popovic, M. Raškovic, J. Upadhyay, and L. Vuškovic, "Plasma Etching of a Single-Cell RF Cavity – Asymmetric Electronegative Discharge", in Proc. SRF'09, Berlin, Germany, Sep. 2009, paper TUPPO083, pp. 427-430.
- [15] L. Zhao, "Surface polishing of niobium for superconducting radio frequency (SRF) cavity applications," Aug. 2014, doi: 10.2172/1287283.
- [16] T Higuchi et al. "Investigation on barrel polishing for superconducting niobium cavity". In: Proc. 7th SRF Int. Workshop, DIST CEA, Gif-sur-Yvette. 1995.
- [17] Tamashevich, Yegor (2017), "Diagnostics and treatment of 1.3 GHz Nb cavities", PhD thesis, Universität Hamburg, 2017, doi:10.3204/PUBDB-2017-00617.
- [18] C. A. Cooper et al., "Integrated Cavity Processing Apparatus at Fermilab: SRF Cavity Processing R&D", in Proc. SRF'11, Chicago, IL, USA, Jul. 2011, paper TUPO025, pp. 424-430.
- [19] C. A. Cooper, B. Bullock, S. C. Joshi, A. D. Palczewski, and K. Saito, "Centrifugal Barrel Polishing (CBP) of SRF Cavities Worldwide", in Proc. SRF'11, Chicago, IL, USA, Jul. 2011, paper WEIOA02, pp. 571-575.
- [20] CA Cooper and LD Cooley. "Mirror-smooth surfaces and repair of defects in superconducting RF cavities by mechanical polishing". In: Superconductor Science and Technology 26.1 (2012), p. 015011.
- [21] Ari Palczewski. R&D progress in SRF surface preparation with centrifugal barrel polishing (CBP) for both Nb and Cu. Tech. rep. Thomas Jefferson National Accelerator Facility, Newport News, VA (United States), 2013.
- [22] George Calota, Natalia Maximova, Katherine S. Ziemer & Sinan Müftü (2009) Investigation of Chemical/Mechanical Polishing of Niobium, Tribology Transactions, 52:4, 447-459, DOI: 10.1080/10402000802687924.
- [23] Calota, G. 2007. "Chemical Mechanical Planarization: A Three Dimensional Mathematical Model and Development of a Process for Polishing Niobium", Masters Thesis, Boston, MA: Northeastern University, Department of Mechanical and Industrial Engineering, 2007.
- [24] Kay Geels et al. Metallographic and materialographic specimen preparation, light microscopy, image analysis, and hardness testing. Vol. 46. ASTM international West Conshohocken, 2007.
- [25] <https://www.lamplan.com/>.
- [26] Kay Geels et al. Metallographic and materialographic specimen preparation, light microscopy, image analysis, and hardness testing. Vol.

46. ASTM international West Conshohocken, 2007, pp. 122-124.
- [27] John Canny. A computational approach to edge detection. *Pattern Analysis and Machine Intelligence*, IEEE Transactions on, (6):679–698, 1986.
- [28] Szeliski, Richard. "Computer vision algorithms and applications." 2011. <http://dx.doi.org/10.1007/978-1-84882-935-0>.
- [29] J. Knobloch and H. Padamsee. "Enhanced susceptibility of Nb cavity equator welds to the hydrogen related Q-virus". In: 8th Workshop on the RF Superconductivity, Padova, Italy. 1998.
- [30] D Ohlendorf and E Wicke. Heat capacities between 1.5 and 16 k and superconductivity of v/h and nb/h alloys. *Journal of Physics and Chemistry of Solids*, 40(10):721–728, 1979.
- [31] HK Birnbaum, ML Grossbeccr, and M Amano. Hydride precipitation in nb and some properties of nbh. *Journal of the Less Common Metals*, 49:357–370, 1976.
- [32] T. Junginger, Investigation of the surface resistance of superconducting materials, Ph.D. thesis, University of Heidelberg, 2012.
- [33] R. Kleindienst, O. Kugeler and J. Knobloch, "Development of an Optimized Quadrupole Resonator at HZB", in Proc. 16th Int. Conf. RF Superconductivity (SRF'13), Paris, France, 2013, TUP074.
- [34] P. B. Welander, M. A. Franzi, and S. G. Tantawi, "Cryogenic RF Characterization of Superconducting Materials at SLAC With Hemispherical Cavities", in Proc. SRF'15, Whistler, Canada, Sep. 2015, paper TUPB065, pp. 735–738.
- [35] G. Martinet, "Results on Bulk Niobium Surface Resistance Measurement With Pillbox Cavity on TE011 and TE012 Modes", in Proc. SRF'19, Dresden, Germany, Jun.-Jul. 2019, pp. 833-837. doi:10.18429/JACoW-SRF2019-THP003.
- [36] D. R. Steinmetz & S. Zaeferrer (2010) Towards ultrahigh resolution EBSD by low accelerating voltage, *Materials Science and Technology*, 26:6, 640-645, DOI: 10.1179/026708309X12506933873828.
- [37] <https://www.hidenanalytical.com/>.
- [38] <https://www.insp.upmc.fr/>.
- [39] <http://www.casaxps.com/>
- [40] https://srdata.nist.gov/xps/main_search_menu.aspx
- [41] Major, George H. et al. "Practical guide for curve fitting in x-ray photoelectron spectroscopy." *Journal of Vacuum Science and Technology* 38 (2020): 061203.
- [42] Matsumoto, Ryo et al. "Reproducibility of XPS analysis for film thickness of SiO₂/Si by active Shirley method." *Journal of Electron Spectroscopy and Related Phenomena* 207 (2016): 55-59.
- [43] Kowalski, Kazimierz. "'IN SITU' XPS INVESTIGATION OF THE BAKING EFFECT ON THE SURFACE OXIDE STRUCTURE FORMED ON NIOBIUM SHEETS USED FOR SUPERCONDUCTING RF CAVITY PRODUCTION." (2003).
- [44] J. Knobloch, "The "Q disease" in Superconducting Niobium RF Cavities", *AIP Conference Proceedings* 671, 133-150 (2003) <https://doi.org/10.1063/1.1597364>.
- [45] Prudnikava, Alena & Tamashevich, Yegor & Yanushkevich, Kazimir & Noei, Heshmat & Lott, D. & Stierle, Andreas & Foster, Brian. (2018). Toward Optimization of Centrifugal Barrel Polishing Procedure for Treatment of Niobium Cavities. *IEEE Transactions on Applied Superconductivity*. PP. 1-1. 10.1109/TASC.2018.2791641.
- [46] Higuchi, T., Saito, K., Yamazaki, Y., Ikeda, T., & Ohgushi, S. (2003). Hydrogen Q-disease and electropolishing (KEK-PROC--2003-2). Japan.
- [47] O. Hryhorenko et al., "Investigation of an Alternative Path for SRF Cavity Fabrication and Surface Processing," in Proc. SRF 2021, East Lansing, MI, USA, pp. 319–322, Jun-Jul 2022.